A high yield rate MEMS gyroscope with a packaged SiOG process

INSTITUTE OF PHYSICS PUBLISHING JOURNAL OF MICROMECHANICS AND MICROENGINEERING

J. Micromech. Microeng. **15** (2005) 2003–2010 doi:10.1088/0960-1317/15/11/003

A high yield rate MEMS gyroscope with a packaged SiOG process

Moon Chul Lee[1], Seok Jin Kang[2], Kyu Dong Jung[1], Sung-Hoon Choa[2] and Yong Chul Cho[2]

[1] Packaging Center, Samsung Advanced Institute of Technology, PO Box 111, Suwon 440-600, Korea
[2] MEMS Lab, Samsung Advanced Institute of Technology, PO Box 111, Suwon 440-600, Korea

E-mail: shchoa@samsung.com

Received 4 April 2005, in final form 14 August 2005
Published 20 September 2005
Online at stacks.iop.org/JMM/15/2003

Abstract

MEMS devices such as a vibratory gyroscope often suffer from a lower yield rate due to fabrication errors and external stress. In the decoupled vibratory gyroscope, the main factor that determines the yield rate is the frequency difference between the sensing and driving modes. The gyroscope, fabricated with a SOI (silicon-on-insulator) wafer and packaged using anodic bonding, has a large wafer bowing caused by thermal expansion mismatch as well as non-uniform surfaces of the structures caused by the notching effect. These effects result in a large distribution in the frequency difference, and thereby a lower yield rate. To improve the yield rate we propose a packaged SiOG (silicon-on-glass) technology. It uses a silicon wafer and two glass wafers to minimize the wafer bowing and a metallic membrane to avoid the notching. In the packaged SiOG gyroscope, the notching effect is eliminated and the warpage of the wafer is greatly reduced. Consequently, the frequency difference is more uniformly distributed and its variation is greatly improved. Therefore, we can achieve a more robust vibratory MEMS gyroscope with a higher yield rate.

(Some figures in this article are in colour only in the electronic version)

1. Introduction

Although MEMS technology is being widely used in these days, successful commercialization of MEMS devices is still one of the major concerns. The difficulty of commercialization arises from several reasons including fabrication imperfections, lack of standardization, complexity of packaging and reliability problems. For example, MEMS vibratory gyroscopes and accelerometers, which use resonators oscillating at their natural resonant frequency, are very sensitive to fabrication errors and external stresses [1]. The fabrication errors not only change the stiffness, but also change the desired dimensions of the resonator, which lead to a change in the natural frequency of the resonator. In addition, the stresses induced during the fabrication process, such as bonding and packaging, cause deformation of the resonator resulting in frequency change or breakage of the resonator [2]. Frequency stability of the resonator can directly affect the performance of the system, that is, a slight frequency shift will lead to a large change in the sensitivity and the phase delay of the output signal. Once the operational frequency range is determined, it is very difficult to adjust or compensate the frequency shift. Even though electronic tuning methods or sophisticated control circuits could be used for compensating the frequency shift [3], it must be minimized during the fabrication process in order to get a better performance and a higher yield rate of the MEMS devices.

Fabrication errors include notching, misalignment, critical dimension (CD) loss, etc. Among them, notching or footing is a well-known problem that is difficult to control and eliminate. Notching is caused by a surface charging effect on the oxide layer at the bottom or sidewall of the trench due to poor charge relaxation and a lack of neutralization by electrons during deep reactive ion etching (DRIE) [4]. Since the etching

rate of DRIE has a strong dependence on the trench width [5], wide trenches are usually overetched when the narrow trenches are etched to the desired dimension. This notching effect will lead to rough and distorted surfaces as well as a non-uniform distribution of mass and stiffness, which can significantly change the design specifications. Although the frequency stability can be optimized, to some extent, by a robust design process [6, 7], it must be minimized during the fabrication process. Furthermore, overetched structures have poor strength and will have more chance of mechanical failure and poor reliability.

Another critical concern affecting the performance and reliability of MEMS is the generation of stress within the structure. External stress in MEMS structures is induced during the fabrication process and the residual stress is generated mainly during the film deposition process. While the residual stress can be minimized by a delicate control of the deposition conditions, the external stress caused by bonding and packaging is inevitable to some extent and difficult to control. For example, wafer level anodic bonding is commonly used to package the MEMS gyroscope structure for its cost advantage and manufacturing efficiencies [8, 9]. It is well known that when glass and silicon are anodically bonded together at a high temperature, thermal stress is produced due to mismatch in the thermal expansion between the silicon and the glass. Consequently, the bonded wafer will have a convex shape from the glass side [10]. This thermomechanical stress will result in a frequency shift of the MEMS gyroscope structures, consequently degrading the performance as well as the yield rate.

In this paper, we describe two critical issues, namely notching and bonding induced stress, and their effects on the frequency shift and yield rate for the vibratory MEMS gyroscope, which is manufactured by a well-known SOI (silicon-on-insulator) process. Then in order to avoid the notching and minimize the external stress, respectively, we propose a novel process technology of the MEMS gyroscope, which utilizes a metal membrane and a packaged SiOG (silicon-on-glass) process. The feasibility of the proposed SiOG gyroscope is verified by comparing the frequency shift, warpage, yield rate and notching with the SOI gyroscope.

2. Vibratory MEMS gyroscope using the SOI process

Figure 1 shows a schematic drawing of the decoupled lateral vibratory MEMS gyroscope considered in this study. It consists of a driving structure and a sensing structure. The driving structure is driven by the comb drive in the x-direction. The sensing structure, connected to the driving structure through the sensing spring, oscillates in the y-direction due to the Coriolis acceleration relative to the driving motion. The independent springs for driving and sensing modes are used to avoid the coupling effect that is caused by the mechanical interference between the driving and the sensing modes. Several authors have reported a similar structure of the MEMS gyroscope [11, 12].

The decoupled vibratory gyroscope shown in figure 1 is fabricated with the SOI wafer, and packaged using the anodic bonding process in vacuum in order to achieve a high quality

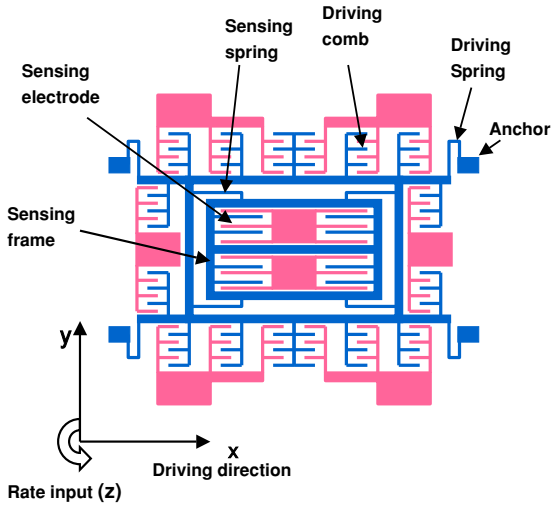

Figure 1. Schematic drawing of the decoupled lateral vibratory MEMS gyroscope.

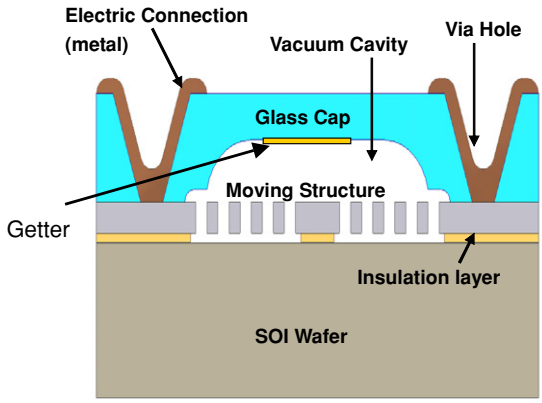

Figure 2. Cross-sectional view of vacuum packaged MEMS gyroscope using the SOI process.

factor (Q-factor). Figure 2 illustrates the cross-sectional view of a vacuum packaged gyroscope consisting of a 4 inch SOI structure wafer and cap glass wafer. The SOI wafer is 500 μm thick with a 3 μm thick insulating SiO_2 layer and a 40 μm thick top silicon layer. The top silicon layer, which is the gyroscope structure, is p-type with (1 0 0) orientation having a resistivity of 0.01–0.02 Ω cm. Inductively coupled plasma reactive ion etching (ICP RIE) is used to vertically etch the silicon layer. Then the final gyroscope structure is released after the sacrificial SiO_2 layer is removed with a wet etch in hydrofluoric acid. The upper cap wafer is Pyrex (Corning 7740) glass of 350 μm thickness. Via holes for feed-through in the glass wafer are fabricated using a sandblasting process. The shallow cavity in glass is fabricated with a wet etching process. Then Ti coating as a getter material is applied by evaporation on the surface of the glass wafer inside the cavity in order to control the Q-factor, that is, to reduce outgassing trapped inside the cavity [13, 14]. Actually, the Ti coating can have two functions. First, a metal coating can function as a diffusion barrier to gas atoms. Second, getter materials, such as titanium, have the ability to absorb common gases when activated at a certain temperature. Therefore, this can reduce the trapped gases

inside the cavity as well as the outgassing generated during the bonding process [14, 15]. Anodic bonding between the SOI wafer and the glass wafer is performed in the vacuum chamber at 5×10^{-5} Torr pressure by applying a high temperature of 460 °C and a dc voltage of about 450 V to the wafers. After bonding is complete, the aluminum film is evaporated on the glass surface to form the contact pads for electric connection, and the bonded wafer is finally diced into 2.7 mm × 2.7 mm gyroscope dies.

The average Q-factor of an individual gyroscope die is measured to be about 3000 for the driving mode and about 300 for the sensing mode. The frequencies of the driving mode and sensing mode are set for 7 kHz and 7.106 kHz, respectively. The yield rate or the performance of the decoupled vibratory gyroscope in the wafer die level is generally determined by four parameters, which are the Q-factor, the resonant frequencies of two modes (driving and sensing modes), and the difference in the resonant frequency of two modes. Among those parameters, however, it was known that the difference in the resonant frequency between the two modes is the key factor in determining the performance of the gyroscope, such as the sensitivity and the bandwidth [7, 16]. Also we found that the frequency difference in the two modes is very difficult to control. Thus, the difference of the two frequencies has to be within a specific range in spite of the fabrication error and the external stresses to increase the yield rate. Although the frequency variation of each mode is large to some extent, the variation of the frequency difference in the two modes should be kept as small as possible. In this study, the targeted frequency difference is set to be 106 ± 70 Hz, which means that the allowable variation in the frequency difference is ranged from 36 Hz (LSL, lower specification limit) to 176 Hz (USL, upper specification limit). Any gyroscope with a range beyond these specification limits will be considered a failed gyroscope. Therefore, in this study, we focused on reducing the variation of the frequency difference to achieve the higher yield rate.

In order to investigate the damage caused by the notching, each comb drive structure and spring in the gyroscope are observed with SEM after the ICP RIE process. Figure 3 shows the SEM pictures of the comb fingers, which were severely damaged by the notching effects. Figure 3(b) shows the bottom surface of the comb drive structure. It has very irregular and rough surfaces. Those non-uniform surfaces of the MEMS structure will increase the variation of the resonant frequency in a wafer. Furthermore, the notching will greatly reduce the stiffness or the strength of the gyroscope structure, resulting in unexpected failure at levels below the specified shock levels during shock or drop tests.

After anodic bonding, the wafer bowing is also measured by measuring the highest and lowest points of the top and bottom surface of the deformed wafer. After dozens of gyroscope wafers are manufactured, the average magnitude of the bonded wafer bowing is found to be about 112 μm with a convex shape of the glass side. Figure 4 shows a typical frequency difference map for each gyroscope die within a wafer. Note that the allowable variation in the frequency difference ranges from 36 to 176 Hz. In this figure, failed and 'bad' gyroscope dies are marked as black and white, respectively. The white dies indicate the gyroscope dies that do not satisfy the targeted specification of the Q-value as well as the resonant frequency of the two modes.

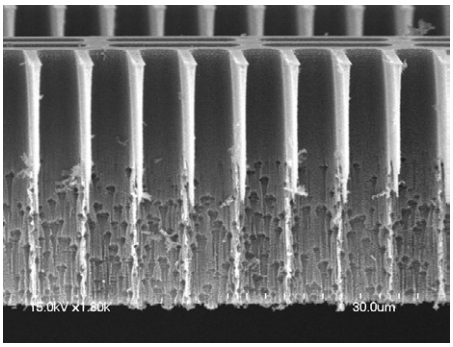

(a)

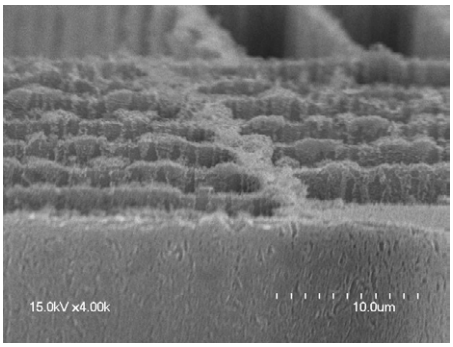

(b)

Figure 3. SEM pictures of (a) severely damaged comb fingers; (b) roughened bottom surface of the comb structure by the notching phenomenon.

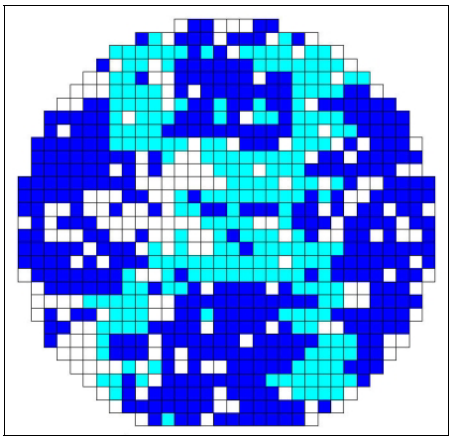

□ : Bad dies which do not satisfy spec. of frequency difference (Δ f) and Q-factor
■ : Dies which do not satisfy spec. of Δ f
■ : Good dies which satisfy spec. of Δ f and Q-factor

Figure 4. The frequency difference map for each gyroscope die within a wafer using the SOI process.

Also the black dies indicate the dies that do not satisfy the targeted specification of the frequency difference. The gray dies indicate 'good' dies that satisfy the specification of the frequency difference as well as the Q-value and the resonant frequency of two modes. In this study, the yield rate is the ratio of the good gyroscope dies among the total gyroscope dies in a wafer that satisfy the targeted specification of all four parameters, namely the Q-value, the frequency of each

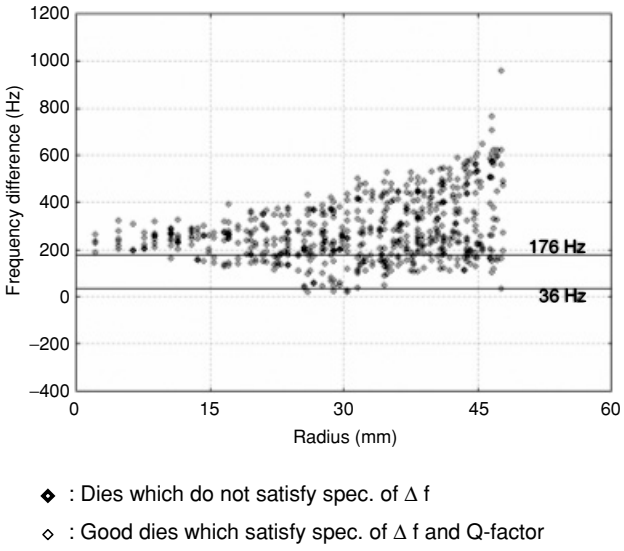

Figure 5. The equiradial distribution of the frequency difference for the gyroscope dies within a wafer with increasing radius.

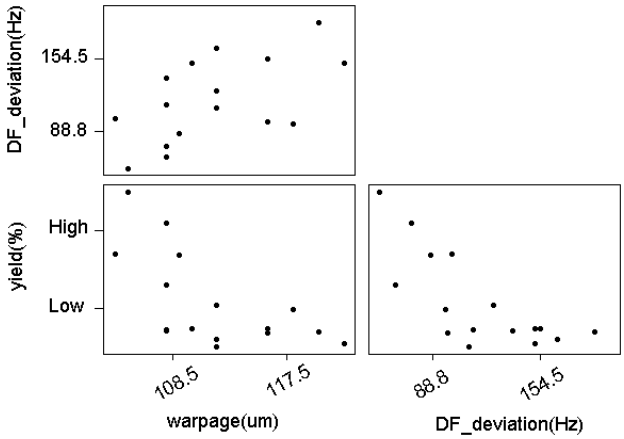

Figure 7. The correlation graphs between warpage, yield rate and standard deviation of the frequency differences (DF_deviation in the figure).

mode and the frequency difference. We found that most of the gyroscopes located in the edge area of the wafer fail and the yield rate of the wafer is very low. Figure 5 shows the equiradial frequency difference distribution of the individual gyroscope dies in radial direction from the center of the wafer. The frequency difference of the gyroscope dies increases with increasing radius, and reaches a maximum value of about 650 Hz at the end of the wafer edge. Figure 6 shows the statistical distribution of the frequency difference for each gyroscope die in a wafer that is marked in black and gray in figure 4. The mean value of the frequency difference is around 190 Hz, and the standard deviation is 174.2 Hz. The frequency differences of the gyroscope dies are between −200 Hz and 650 Hz.

After dozens of the gyroscope wafers were manufactured and tested, it was found that the wafer bowing is closely correlated with the variation in the frequency difference of the gyroscope die. Figure 7 shows the measured data for the relationship between the wafer bowing and the standard deviation of the frequency difference. From the figure, we can see that larger wafer bow results in a larger standard deviation of the frequency difference. This depicts that larger wafer bowing induces larger stress on the bonded wafer [17]. The relation between the yield rate of the gyroscope die in the wafer and the wafer bowing is investigated next. As shown in figure 7, the yield rate of the gyroscope is closely correlated with the wafer bowing. The larger the wafer bowing the lower the yield rate of the gyroscope die. It is also found that the yield rate of most of the gyroscopes fabricated with the SOI process is very low. For example, even the 'high' yield rate shown in figure 7 represents the yield rate of less than 50%. In conclusion, it is obvious that larger variation of the frequency difference for the SOI gyroscope is attributed to the wafer bowing as well as the notching effect.

Thus, the wafer warpage and the notching are the key parameters determining the yield rate of the gyroscope, and these parameters should be reduced to achieve the higher yield rate. In this study, a novel design that can reduce the wafer bowing as well as the notching is presented.

3. SiOG gyroscope fabrication process

The developed process in this paper is based on a packaged SiOG technology, which uses a silicon wafer and two glass

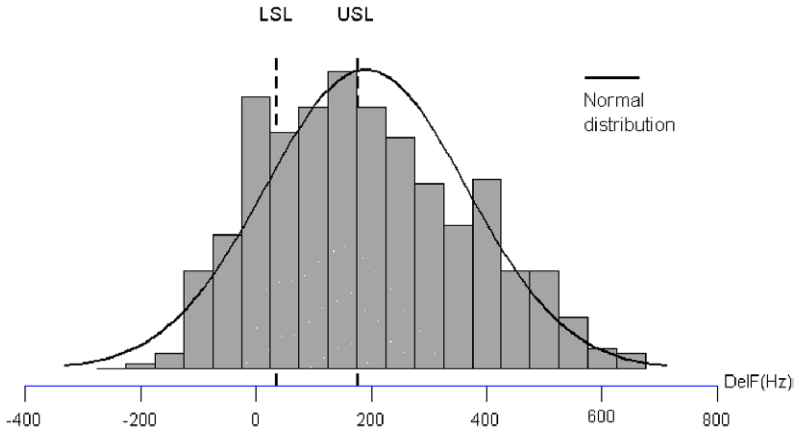

Figure 6. The statistical distribution of frequency difference of each gyroscope die in a wafer using the SOI process.

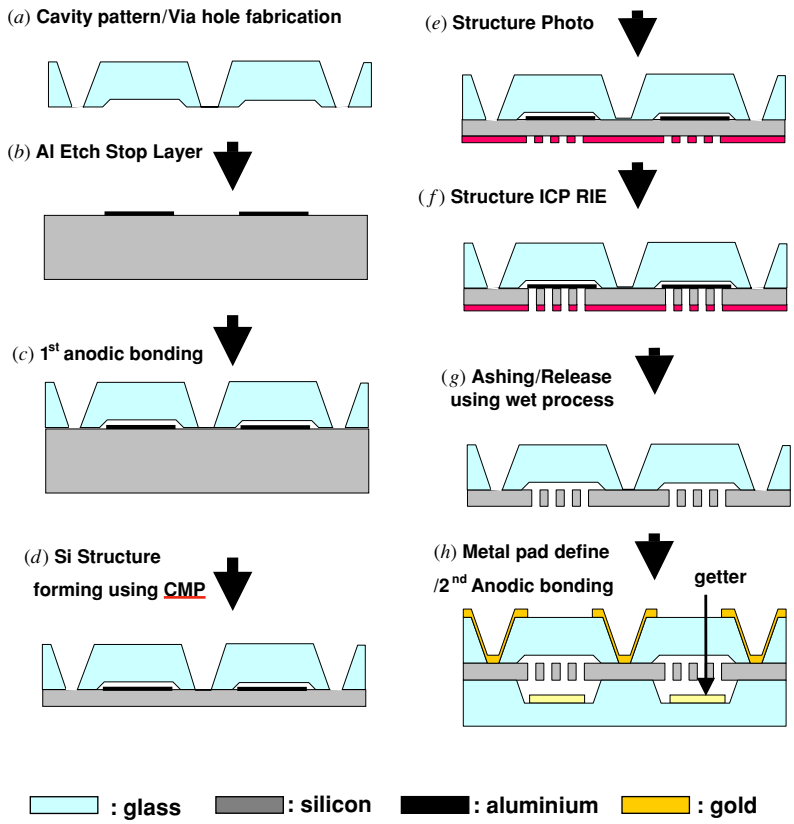

Figure 8. Fabrication process of a packaged SiOG gyroscope.

wafers. The gyroscope fabrication processes using the packaged SiOG technology are shown in figure 8. The fabrication process of the gyroscope structure is very similar to the SOI process except that the packaged SiOG process uses the two-step anodic bonding process along with the metal membrane. The top glass wafer of 350 μm thickness is prepared. The via hole for feed-through of the glass wafer is fabricated with the sandblaster process, and the cavity of 25 μm depth is fabricated with a wet etch in hydrofluoric acid. In figure 8(b) an aluminum layer of 2 μm thickness is deposited on the silicon wafer as an etch stop layer. Another important function of the aluminum layer is to prevent the notching phenomenon during the ICP RIE process. After anodic bonding between the top glass wafer and the silicon structure wafer, the silicon structure wafer is lapped and polished to 40 μm thickness by chemical mechanical polishing (CMP). The anodic bonding conditions used in the SiOG process are identical to those in the SOI process, namely temperature of 460 °C and voltage of 450 V. The movable gyroscope structure is fabricated by photolithography and the ICP RIE etching process as shown in figure 8(f). The aluminum layer and residue of the photo-resist are removed with sulfuric acid and the ashing process, respectively. The bottom glass of 350 μm thickness is also prepared separately. A cavity of 160 μm depth in the bottom glass is fabricated with a wet etching process. A Ti coating is also applied inside the cavity in order to control the Q-factor. As a final step, the second anodic bonding is performed between the silicon structure in figure 8(g) and the bottom glass wafer. Figure 8(h) illustrates the cross-sectional view of a vacuum-packaged gyroscope fabricated with the packaged SiOG process.

4. Experimental results and discussion

Figure 9 shows the SEM pictures of the fabricated comb drive fingers after the ICP RIE process. The bottom area of the comb drive structure is not damaged, and the sidewall surface profile is flat and clean as the polished surface. A sharp silhouette of the comb fingers indicates that there is no evidence of plasma damage. This indicates the effectiveness of the aluminum layer in achieving the notch-free structures. Since the aluminum metal layer does not get charged, it does not deflect impinging ions toward silicon at the sidewall; therefore, notching does not take place. In addition, the aluminum layer will enhance the heat dissipation throughout the wafer during the ICP RIE process. It is known that the ICP RIE process is sensitive to temperature change; when temperature increases, sidewall passivation effects deteriorate [18]. In this study, we experienced that the gyroscope structures are frequently distorted or deformed after the ICP RIE process without the metal membrane. It is thought that during the ICP etching process, the generated heat is concentrated on a localized area such as the neck area of the comb structures in the electrodes since the gyroscope structures are isolated from the bottom surface. With the aluminum layer, therefore, heat will be dissipated more efficiently with conduction throughout the whole wafer, which prevents degradation of polymer passivation as well as distortion of the gyroscope structures.

Table 1. The measured wafer bowing during each packaged SiOG fabrication.

	Packaged SiOG fabrication process in figure 8	Wafer bowing (μm)
Figure 8(a)	Top glass wafer of 350 μm thickness	$-20 \sim -100$
Figure 8(b)	Silicon wafer of 500 μm thickness	+15
Figure 8(c)	First anodic bonding of each wafer	+110
Figure 8(d)	CMP process of silicon wafer up to 40 μm	+170
Figure 8(h)	Second anodic bonding between top glass wafer (350 μm) with Si wafer (40 μm) and bottom glass wafer (350 μm)	-10

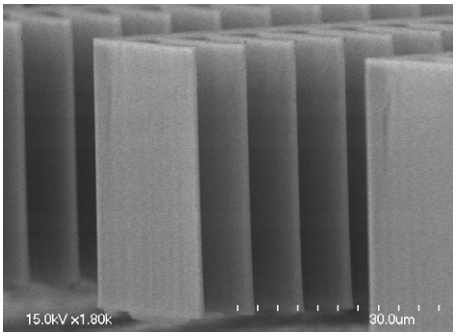

(a)

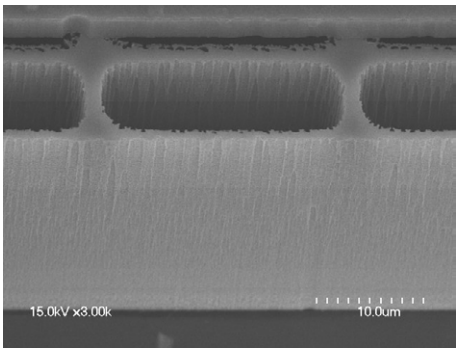

(b)

Figure 9. SEM pictures of (a) comb drive fingers, (b) bottom surface of the comb drive structure fabricated with the metal membrane.

Another important advantage of the packaged SiOG process used in this study is the dramatic reduction of the wafer warpage. Table 1 shows the magnitude of the wafer bowing measured for each fabrication process. In the table the '+' sign represents the convex shape of the wafer bowing. In figure 8(a), the top glass wafer exhibits concave bowing, which varies from -20 μm to -100 μm. The silicon wafer after deposition of the aluminum layer has a convex bowing of +15 μm. In figure 8(c), after anodic bonding between the glass wafer and the silicon wafer, the bonded wafer is bowed by +110 μm, which is a glass convex shape. Then the wafer bowing of the bonded wafer becomes +170 μm when the silicon wafer is fabricated with the CMP process up to a thickness of 40 μm as shown in figure 8(d). In figure 8(h), after final anodic bonding between the bonded wafer in figure 8(d) and the bottom glass wafer, the wafer bowing becomes -10 μm. This is a dramatic reduction in the wafer warpage compared to the SOI wafer process, which has an average warpage of +112 μm.

After completion of the packaged SiOG fabrication, the frequency difference was measured for all gyroscope dies in a wafer. Figure 10 shows the equiradial frequency difference distribution of the gyroscope dies in the radial direction. It is observed that the frequency difference is more uniformly distributed throughout the whole wafer and shows almost no change with increasing radius compared with that of the SOI gyroscope in figure 2. Figure 11 shows the statistical distribution of the frequency difference for each gyroscope die that satisfies the specification of the Q-value and the resonant frequency of the two modes. The frequency difference of the gyroscope dies ranges from -50 Hz to 250 Hz, which exhibits a great improvement compared with that of the SOI gyroscope. It indicates that more gyroscopes in a wafer meet the target specification of the frequency difference. The mean and standard deviation values of the frequency difference are 102 and 51.4 Hz, respectively. In conclusion, the SiOG gyroscope shows a much higher yield rate than the SOI gyroscope. We could achieve the vibratory gyroscope of the higher yield rate by utilizing the metal membrane and the packaged SiOG process.

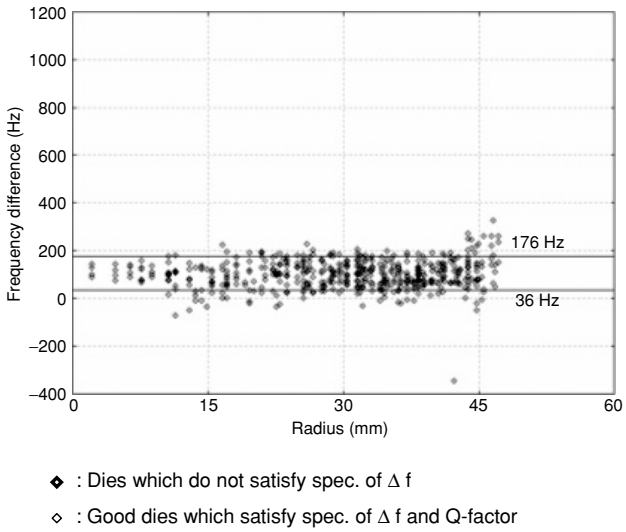

Figure 10. The equiradial distribution of the frequency difference for the gyroscope dies within a wafer with increasing radius.

Another possible method to reduce the wafer warpage could be to lower the anodic bonding temperature. We found that the wafer bowing decreases with a reduction in bonding temperature as shown in figure 12, when anodic bonding is performed between the glass wafer of 350 μm thickness and the silicon wafer of 500 μm thickness. For example, when we conducted the anodic bonding with a temperature of 340 °C, we could achieve the wafer bowing of 17 μm. However, anodic bonding with lower temperature resulted in failure of the vacuum state inside the cavity of the gyroscope.

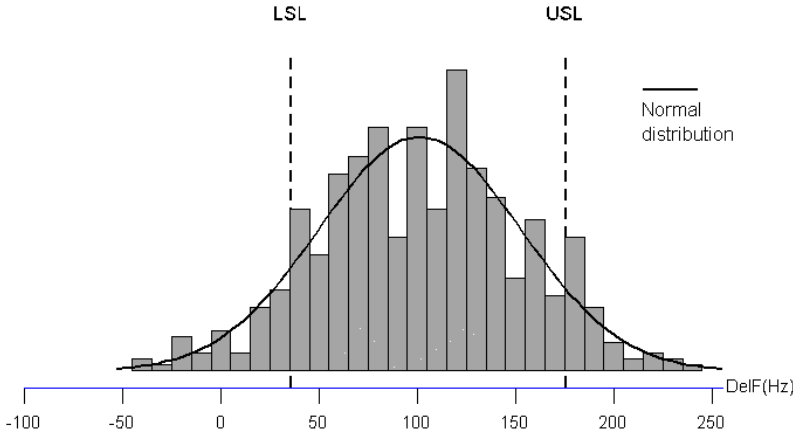

Figure 11. The statistical distribution of frequency difference of the gyroscope dies within a wafer using the packaged SiOG process.

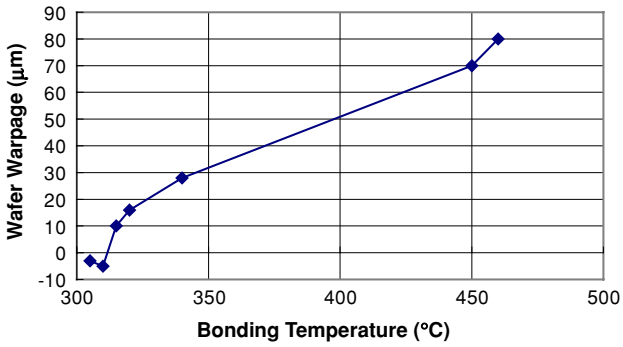

Figure 12. Wafer warpage of the anodically bonded wafer with increasing bonding temperature.

We found that the Q-factor of the gyroscope, which indicates vacuum integrity, dramatically reduced during environmental reliability tests. It is thought that lower bonding temperature will reduce the bonding strength, which tends to produce defects or voids in the bonding interface, thereby increasing the chance of leakage. Therefore, we could not apply a lower bonding temperature to reduce the wafer bowing in this study.

5. Conclusions

In this paper, we describe two critical issues, namely the notching and the bonding induced stress, and study their effects on the yield rate and the performance for the vibratory MEMS gyroscope. The decoupled vibratory gyroscope is fabricated with a SOI wafer, and packaged using the anodic bonding. The SOI gyroscope has a large wafer bowing of 112 μm as well as the non-uniform surfaces of the structures damaged by the notching effect, which cause a larger distribution in the frequency difference. It is found that the wafer bowing, the frequency difference and the yield rate of the gyroscope in the wafer are closely correlated. As the wafer bowing becomes larger, the variation in the frequency difference becomes larger; consequently, the yield rate becomes lower. Therefore, the SOI gyroscope shows a very low yield rate. We then propose a packaged SiOG technology that uses a silicon wafer and two glass wafers to minimize the wafer bowing. With the packaged SiOG gyroscope, the warpage of the wafer is greatly reduced to 10 μm. We also utilize the aluminum membrane to avoid the notching and to enhance the heat dissipation throughout the wafer during the ICP RIE process. Therefore, the notch-free and more robust structures are obtained. Consequently the frequency difference is more uniformly distributed, and the standard deviation of the frequency difference becomes 51.4 Hz compared with 174.2 Hz for the SOI gyroscope. Therefore, we could achieve a vibratory MEMS gyroscope that has a higher yield rate and greater robustness.

References

[1] Liu R L, Paden B and Turner K 2002 MEMS resonators that are robust to process-induced feature width variations *J. Microelectromech. Syst.* **11** 403–8
[2] Li G and Tseng A 2001 Low stress packaging of a micromachined accelerometer *IEEE Trans. Electron. Packag. Manuf.* **24** 18–25
[3] Painter C C and Shkel A M 2003 Active structural error suppression in MEMS vibratory rate integrating gyroscopes *IEEE Sensors J.* **3** 595–606
[4] Ishihara K, Yung C F, Ayon A A and Schmidt M A 1999 An inertial sensor technology using DRIE and wafer bonding with interconnecting capability *J. Microelectromech. Syst.* **8** 403–8
[5] Fu L, Miao J M, Li X X and Lin R M 2001 Study of deep silicon etching for micro-gyroscope fabrication *Appl. Surf. Sci.* **177** 78–84
[6] Han J S and Kwak B M 2001 Robust optimal design of a vibratory microgyroscope considering fabrication errors *J. Micromech. Microeng.* **11** 662–71
[7] Hwang K H, Lee K H, Park G J, Lee B L, Cho Y C and Lee S H 2003 Robust design of a vibratory gyroscope with an unbalanced inner torsion gimbal using axiomatic design *J. Micromech. Microeng.* **13** 8–17
[8] Ko W H, Suminto J T and Yeh G J 1985 *Bonding Techniques for Microsensor: Micromachining and Micropackaging of Transducers* (Amsterdam: Elsevier) pp 41–61
[9] Li Z, Hao Y, Zhang D, Li T and Wu G 2002 An SOI-MEMS technology using substrate layer and bonded glass as wafer-level package *Sensors Actuators* A **96** 34–42
[10] Rogers T and Kowal J 1995 Selection of glass, anodic bonding conditions and material compatibility for silicon-glass capacitive sensors *Sensors Actuators* A **46–47** 113–20
[11] Oh Y S, Lee B L, Baek S S, Kim H S, Kim J G, Kang S J and Song C M 1998 A tunable vibratory microgyroscope *Sensors Actuators* A **64** 51–6
[12] Lee B L, Lee S W, Jung K D, Choi J H, Chung T R and Cho Y C 2001 A de-couple vibratory gyroscope using a

mixed micro-machining technology *Proc. IEEE Int. Conf. on Robotics Automation (Seoul)* pp 3412–6
[13] Mack S, Baumann H, Gösele U, Werner H and Schlögl R 1997 Analysis of bonding-related gas enclosure in micromachined cavities sealed by silicon wafer bonding *J. Electrochem.* **144** 1106–10
[14] Minami K, Moriuchi T and Esashi M 1995 Cavity pressure control for critical damping of packaged micro mechanical devices *Transducer'95 8th Int. Conf. on Solid-State Sensors and Actuators (Stockholm)* pp 240–3
[15] Moraja M and Amiotti M 2003 Getters films at wafer level for wafer to wafer bonded MEMS *Symp. on Design, Test, Integration Packaging of MEMS/MOEMS* pp 346–9
[16] Baek S S, Oh Y S, Ha B J, An S D, An B H, Song H and Song C M 1999 A symmetrical z-axis gyroscope with a high aspect ratio using simple and new process *12th IEEE Int. Conf. MEMS'99* pp 612–7
[17] Hsu T R 2004 *MEMS Packaging (EMIS Processing Series No. 3: Inspec Press)* pp 33–7
[18] Sun Y, Piyabongkarn D, Sezen A, Nelson B J and Rajamani R 2002 A high-aspect-ratio two-axis electrostatic microactuator with extended travel range *Sensors Actuators* A **102** 49–60